Site-selective doping effect in AMn(3)V(4)O(12) (A = Na(+), Ca(2+), and La(3+)).

ARTICLE *in* JOURNAL OF THE AMERICAN CHEMICAL SOCIETY · OCTOBER 2012

Impact Factor: 12.11 · DOI: 10.1021/ja308851f · Source: PubMed

JACS
JOURNAL OF THE AMERICAN CHEMICAL SOCIETY
Article
pubs.acs.org/JACS

Site-Selective Doping Effect in $AMn_3V_4O_{12}$ (A = Na^+, Ca^{2+}, and La^{3+})

Shoubao Zhang,[†] Takashi Saito,[†] Masaichiro Mizumaki,[‡] Wei-tin Chen,[†] Takenori Tohyama,[†] and Yuichi Shimakawa*[,†,§]

[†]Institute for Chemical Research, Kyoto University, Uji, Kyoto 611-0011, Japan
[‡]Japan Synchrotron Radiation Research Institute, SPring-8, 1-1-1 Kouto, Sayo-cho, Sayo-gun, Hyogo 679-5198, Japan
[§]Japan Science and Technology Agency, CREST, Uji, Kyoto 611-0011, Japan

ABSTRACT: A-site-ordered perovskite-structure oxides with Mn and V at A′ and B sites, respectively, were synthesized by using a high-pressure method. Valence-state analyses revealed that the A-site substitution modulated the valence states of the Mn ions at the A′ site and V ions at the B site sequentially. By changing the A-site ions from Na^+ to Ca^{2+} and from Ca^{2+} to La^{3+}, the valence distribution changed site-selectively from $Na^+Mn^{2.33+}{}_3V^{4+}{}_4O_{12}$ to $Ca^{2+}Mn^{2+}{}_3V^{4+}{}_4O_{12}$ and to $La^{3+}Mn^{2+}{}_3V^{3.75+}{}_4O_{12}$. The electrons of the A′-site Mn were localized and contributed to the magnetic properties, that is, spin-glass-like behavior in $NaMn_3V_4O_{12}$ and antiferromagnetic behavior in $CaMn_3V_4O_{12}$ and $LaMn_3V_4O_{12}$. The valence electrons of the B-site V, in contrast, were delocalized, as could be seen from the low resistivity of the samples. The delocalized electrons at the B-site V did not correlate with the localized spins at the A′-site Mn.

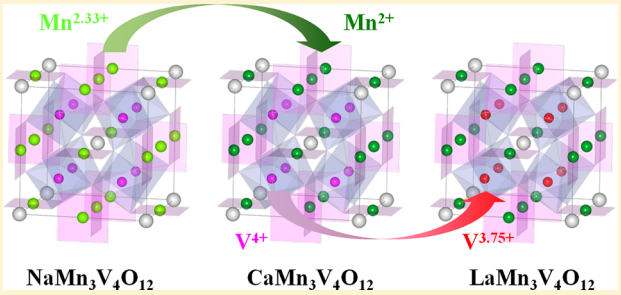

INTRODUCTION

Changing the valence state of transition-metal ions is key to controlling the chemical and physical properties of transition-metal oxides. Chemical doping is the conventional way of modulating the valence states of the transition-metal ions. In ABO_3 perovskite, for example, substitution of ions such as alkaline, alkaline earth, and rare earth ions at the A site is often used for such doping, and the modulated valence states of the transition-metal ions at the B site play an essential role in giving rise to some intriguing properties such as high-T_c superconductivity in cuprates and colossal magnetoresistance in manganates.[1,2] In A-site-ordered perovskites $AA'_3B_4O_{12}$, in which A- and A′-site cations are ordered at an originally 12-fold-coordinated A site in simple ABO_3, there is an extra valence-variable transition-metal ion at the A′ site (see the crystal structure in Figure 1). The valence variations of transition-metal ions at two crystallographic sites and possible interactions between the transition-metal ions like A′−A′ and A′−B as well as B−B would lead to a rich variety of chemical and physical properties.[3,4]

Certain A-site-ordered perovskites show intriguing effects of A-site substitution. For instance, $CaCu_3Mn_4O_{12}$ with the ionic formula $Ca^{2+}Cu^{2+}{}_3Mn^{4+}{}_4O_{12}$ is a semiconductor, and it possesses ferrimagnetism originating from the antiferromagnetic interaction between the spins of A′-site Cu^{2+} and B-site Mn^{4+}.[5] Substitution of Ca^{2+} with La^{3+} or Bi^{3+} at the A site produces $(La/Bi)^{3+}Cu^{2+}{}_3Mn^{3.75+}{}_4O_{12}$, and the resulting compounds are ferrimagnetic metals with spin-polarized conduction carriers. Moreover, low-field magnetoresistance has been observed in $(La/Bi)Cu_3Mn_4O_{12}$ at temperatures below 350 K.[6,7] An analogue compound $CaCu_3Fe_4O_{12}$ can also be synthesized at high pressure and high temperature. The ionic formula is described as $Ca^{2+}Cu^{2+}{}_3Fe^{4+}{}_4O_{12}$, and an unusually high valence state, that is, iron Fe^{4+}, is stable at room temperature. The material shows charge disproportionation to $Ca^{2+}Cu^{2+}{}_3(Fe^{3+}{}_2Fe^{5+}{}_2)O_{12}$ at 210 K, and large ferrimagnetic moments of the A′-site $Cu^{2+}(\uparrow)$ spins and the B-site $Fe^{3+}(\downarrow)Fe^{5+}(\downarrow)$ spins appear concomitantly.[8] Substitution of La^{3+}/Bi^{3+} at the A site changes the compound into $(La/Bi)^{3+}Cu^{2+}{}_3Fe^{3.75+}{}_4O_{12}$ and leads to a completely different behavior at low temperature, that is, intersite charge transfer.[9,10]

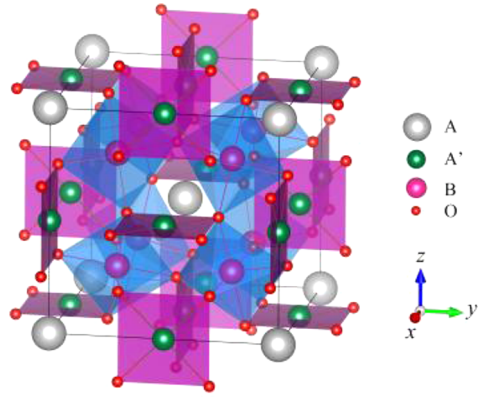

Figure 1. Crystal structure of A-site-ordered perovskite $AA'_3B_4O_{12}$.

Received: September 6, 2012

   dx.doi.org/10.1021/ja308851f | J. Am. Chem. Soc. XXXX, XXX, XXX−XXX

At the intersite charge transfer transition temperature, electrons transfer from the A′-site Cu ion to the B-site Fe ion (ligand holes move from the B-site Fe to the A′-Cu site), and the ionic formula changes from high-temperature $Ca^{2+}Cu^{2+}{}_3Fe^{3.75+}{}_4O_{12}$ to low-temperature $Ca^{2+}Cu^{3+}{}_3Fe^{3+}{}_4O_{12}$, and there are large changes in the structural, magnetic, and transport properties.[11]

In the above A-site-ordered perovskites, aliovalent substitution at the A sites results in doping into the B-site ions. On the other hand, doping into the A′-site ion as well as the B-site ion is also found in $ACu_3V_4O_{12}$ (A = Na^+, Ca^{2+}, and Y^{3+}). By changing the A-site ions, the valences of both the A′-site Cu and the B-site V change. The three compounds are Pauli-paramagnetic metals, and both the A′-site Cu and the B-site V orbitals contribute to metallic conduction. Doping by the A-site substitution shifts the Fermi level in a rigid-band electronic structure to a higher energy.[12] Therefore, the effect of A-site substitution in an A-site-ordered perovskite-structure oxide containing V at the B site is different from that of the A-site substitution in the compounds containing Mn or Fe at the B site.

In this study, we focused on A-site-ordered perovskite oxides containing Mn at the A′ site and V at the B site to see the effect of the A-site substitution. We succeeded in preparing a series of new compounds, $AMn_3V_4O_{12}$ (A = Na^+, Ca^{2+}, and La^{3+}), by using a high-pressure synthesis method, and found a site-selective doping effect into the A′ or B site. The results of structural, magnetic, and transport measurements revealed that the doped electrons of the A′-site Mn ions are localized and responsible for the magnetic properties, while those of the B-site V ions are delocalized and contribute to the conducting properties of the samples.

EXPERIMENTAL SECTION

$AMn_3V_4O_{12}$ (A = Na^+, Ca^{2+}, and La^{3+}) samples were prepared in solid-state reactions under high-temperature and high-pressure conditions. Stoichiometric amounts of the raw materials, Na_2O_2, CaO, La_2O_3, Mn_2O_3, V_2O_3, and V_2O_5, were mixed, packed into gold capsules, placed in a cubic-anvil-type high-pressure apparatus, and treated under 7 GPa for $NaMn_3V_4O_{12}$ and 9 GPa for $CaMn_3V_4O_{12}$ and $LaMn_3V_4O_{12}$ at 900 °C for 30 min. They were quenched to room temperature before the pressure was released.

To identify phase and structure, synchrotron X-ray powder diffraction (SXRD) with a wavelength of λ = 0.5 Å was performed at room temperature at BL19B2 in SPring-8. Powder samples were put into glass capillary tubes and rotated during the measurements, and the diffraction patterns were collected with a large Debye−Scherrer camera. The crystal structures were refined with the Rietveld method and the program GSAS.[13,14] The valence states of Mn and V were investigated at BL25SU in SPring-8 by performing X-ray absorption spectroscopy (XAS) measurements at 14 K using a total electron yield method. The incident photon energy was calibrated by measuring the energies of the Ti-$L_{3,2}$ edges of TiO_2 and the Ni-$L_{3,2}$ edges of NiO. The powder samples were pasted uniformly on a sample holder by using carbon tape.

The magnetic susceptibility of the samples was measured with a magnetic property measurements system (MPMS), Quantum Design, with an RSO method in zero-field-cooling (ZFC) and field-cooling (FC) modes. Resistivity measurements were carried out in a physical property measurements system (PPMS), Quantum Design, by using the four-probe method.

RESULTS AND DISCUSSION

The resulting black samples, $NaMn_3V_4O_{12}$ (NMVO), $CaMn_3V_4O_{12}$ (CMVO), and $LaMn_3V_4O_{12}$ (LMVO), were all well crystallized with the A-site-ordered perovskite structures and contained small amounts of VO_2 and $Mn_2V_2O_7$ impurities. Figure 2 shows the SXRD patterns of $AMn_3V_4O_{12}$ (A = Na, Ca, and La) and the structure refinement results of the Rietveld analysis. The refinement revealed that the total amount of impurities was less than 4% in each sample. The main phase of each $AMn_3V_4O_{12}$ was a cubic A-site-ordered perovskite with a space group $Im\bar{3}$, in which A, Mn, V, and O atoms are placed at the 2*a* (0, 0, 0), 6*b* (0, 1/2, 1/2), 8*c* (1/4, 1/4, 1/4), and 24*g* (*x*, *y*, 0) positions, respectively. In the refinements, no vacancies were detected at any of the sites, so the site-occupation factors *g* were fixed at 1. Because the high-pressure synthesis was conducted as a confined reaction in a gold capsule and the resultant samples contained few impurities, the obtained samples should have had almost stoichiometric chemical compositions. The refined structural parameters and selected bond lengths and angles are listed in Table 1. The lattice parameter increases when the A-site ions change from Na to La, and, accordingly, the Mn−Mn distance and the V−O−V bond angle also increase. We estimated the valence states of cations, that is, bond valence sums (BVS) from the refined structural parameters (Table 1). In going from NMVO to CMVO, the BVS of the A′-site Mn decreases, while BVS of the B-site V does not change so much. In going from CMVO to LMVO, in contrast, the BVSs of the A′-site Mn are both close to +2, whereas that of the B-site V decreases significantly. In CMVO, the BVSs for Mn and V are close to +2 and +4, indicating, as expected, the ionic composition of the sample is very close to $Ca^{2+}Cu^{2+}{}_3Mn^{4+}{}_4O_{12}$.

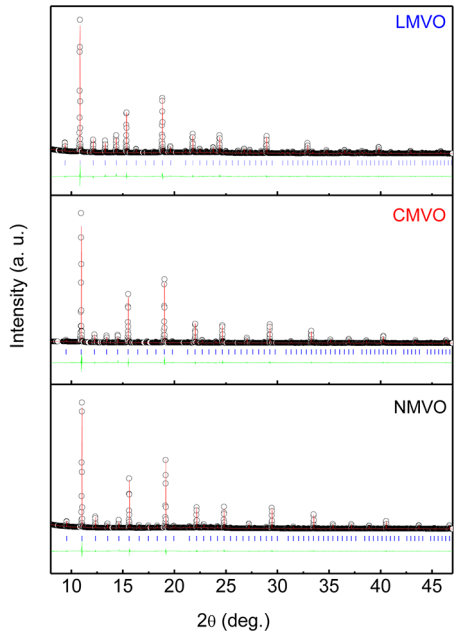

Figure 2. SXRD patterns and the structure refinement results for NMVO, CMVO, and LMVO. The observed (circles), calculated (line), and difference (bottom line) patterns were shown. The ticks indicate the positions of Bragg reflections.

The XAS spectra of the V-*L* (515−520 eV), O-*K* (528−532 eV), Mn-L_2 (638−642 eV), and Mn-L_3 (650−653 eV) edges are shown in Figure 3. The O-*K* edge spectra around 530 eV mainly reflect the features of the electronic structure of V ions at the B site. As shown in Figure 3a, the spectra of NMVO and CMVO are quite similar to each other, while the LMVO spectrum is different from them. The observed V-*L* and O-*K*

dx.doi.org/10.1021/ja308851f | J. Am. Chem. Soc. XXXX, XXX, XXX−XXX

Table 1. Refined Structural Parameters and Selected Bond Lengths and Angles of NMVO, CMVO, and LMVO[a]

	NMVO	CMVO	LMVO
a (Å)	7.35514(4)	7.40704(3)	7.48485(4)
O_x	0.3023(3)	0.2944(3)	0.2947(3)
O_y	0.1917(3)	0.1936(3)	0.1957(3)
U_{iso} (100 × Å^2) for Mn	1.04(2)	1.58(3)	2.04(9)
U_{iso} (100 × Å^2) for V	0.33(1)	0.35(1)	0.27(2)
U_{iso} (100 × Å^2) for O	0.54(3)	0.42(3)	0.65(6)
R_{wp} (%)	4.31	5.84	4.67
R_p (%)	3.05	3.41	3.40
Mn−O (Å)	2.032(2) × 4	2.092(2) × 4	2.124(3) × 4
	2.695(2) × 4	2.733(2) × 4	2.753(2) × 4
	3.169(2) × 4	3.147(2) × 4	3.170(2) × 4
V−O (Å)	1.9248(6) × 6	1.9265(4) × 6	1.9439(6) × 6
V−O−V (deg)	145.6(1)	147.98(9)	148.6(1)
BVS for Mn	2.56	2.11	2.01
BVS for V	4.03	4.04	3.85

[a]Numbers in parentheses are standard deviations of the last significant digit. BVSs for Mn at the A′ site and V at the B site are also listed.

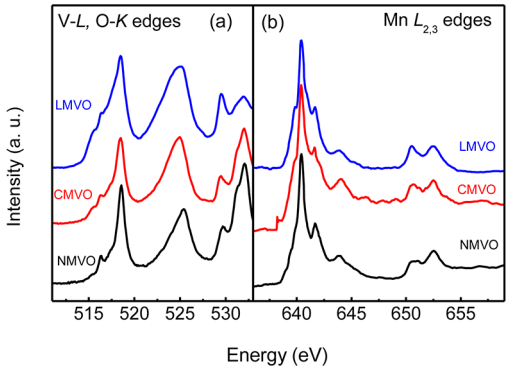

Figure 3. XAS spectra of (a) V-L and O-K edges, and (b) Mn-$L_{2,3}$ edges of NMVO, CMVO, and LMVO.

edge spectra of NMVO and CMVO are very similar to the typical one of V^{4+} in oxides,[15] confirming that the valence states of V ions in the compounds are +4. The V-2p spectrum (~518 eV) of LMVO, in contrast, is much broader than those of NMVO and CMVO, and the broad spectral shape is similar to that of $Y_{1-x}Ca_xVO_3$,[16] in which electrons are doped into the V site, as in $V^{(3+x)+}$. In addition, the peaks of LMVO around 532 eV, which reflect the nature of V-3d bands, are suppressed as compared to those of NMVO and CMVO. These results thus indicate that the valence states of V in LMVO decrease from +4. The above V-L edge XAS results, therefore, strongly suggest that the valence states of V in NMVO and CMVO are close to +4, and the valence state of V in LMVO is less than +4.

On the other hand, in Figure 3b, the XAS spectra at the Mn-$L_{2,3}$ edges for CMVO and LMVO are very similar to each other, whereas the spectrum at the Mn-$L_{2,3}$ edges for NMVO is rather different. The CMVO and LMVO spectra suggest that the ionic state of the Mn ions is very close to that of +2.[17] The NMVO spectrum, in contrast, has typical features of a mixed valence state $Mn^{(2+x)+}$; the shoulder structure of the peak at 640 eV is suppressed, the peak at 642 eV is broad, and the intensity of the peak at 653 eV increases.[17] Therefore, the valence states of Mn in CMVO and LMVO are close to +2, whereas the valence state of Mn in NMVO is higher, that is, $+(2 + x)$.

From the results of structure refinements and XAS spectra analysis, we can conclude that the most plausible ionic formulas for the samples would be $Na^+Mn^{2.33+}{}_3V^{4+}{}_4O_{12}$, $Ca^{2+}Mn^{2+}{}_3V^{4+}{}_4O_{12}$, and $La^{3+}Mn^{2+}{}_3V^{3.75+}{}_4O_{12}$. In NMVO, the A′-site Mn has a mixed valence state. By changing the A-site ions from Na^+ to Ca^{2+}, electrons are doped only into A′-site Mn, and the compound changes into $Ca^{2+}Mn^{2+}{}_3V^{4+}{}_4O_{12}$ with typical ionic states of Mn^{2+} and V^{4+} at the A′ and B sites, respectively. Subsequent change of the A-site ion from Ca^{2+} to La^{3+} causes the electron to be doped only into the B-site V instead of the A′-site Mn. Regarding the change of A-site ions from Na^+ to Ca^{2+} to La^{3+} in the present AMVO system, therefore, the electrons are first doped into the A′-site Mn and then into the B-site V, and selective doping into two different cation sites takes place through the A-site substitution.

Figure 4a shows the temperature-dependent magnetic susceptibility of $AMn_3V_4O_{12}$ (A = Na^+, Ca^{2+}, and La^{3+})

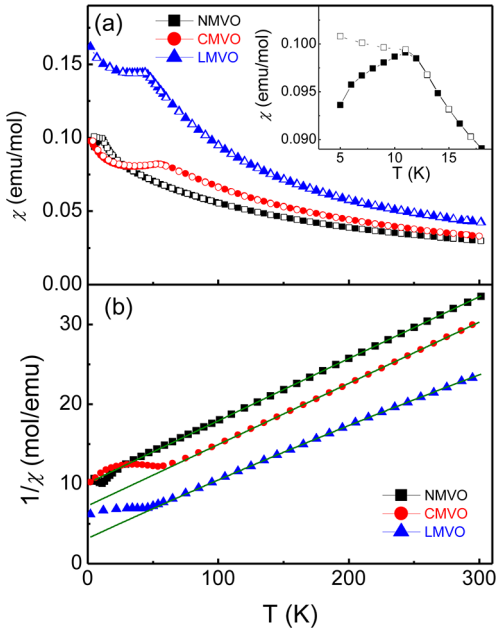

Figure 4. Temperature dependence of (a) susceptibility χ and (b) inverse susceptibility χ^{-1} of NMVO, CMVO, and LMVO. The results of the Curie−Weiss fit (lines) are also shown in (b). The inset of (a) shows ZFC (■) and FC (□) susceptibility curves of NMVO at low temperature.

measured at an applied magnetic field of 1000 Oe. The three samples show Curie−Weiss-like paramagnetic behavior at high temperature and magnetic transitions at low temperature. The high-temperature susceptibility can be fitted by the Curie−Weiss law, $\chi = \chi_0 + C/(T - \theta)$. The fits for the inverse susceptibility are shown in Figure 4b, and the obtained fitting parameters are listed in Table 2. Note that the Weiss temperatures, θ, are negative for the three samples, suggesting antiferromagnetic interactions of the constituent spins. In NMVO, the magnetic susceptibility has a peak at about 11 K, and below this temperature, the susceptibilities measured under FC and ZFC modes show significant differences (inset of Figure 4a), suggesting typical spin-glass-like behavior.[18] The rather high Weiss temperature (−114.62 K) relative to the observed transition temperature indicates that the spins in

dx.doi.org/10.1021/ja308851f | J. Am. Chem. Soc. XXXX, XXX, XXX−XXX

Table 2. Experimentally Obtained Curie–Weiss Parameters of NMVO, CMVO, and LMVO[a]

AMVO	NMVO	CMVO	LMVO
χ_0 (emu/mol)	0.0017	0.00003	0.0048
θ (K)	−114.62	−98.94	−41.05
C (emu K/mol)	11.71	12.79	12.75
C_{cal}^{Mn} (emu K/mol)	11.76 ($2Mn^{2+} + Mn^{3+}$)	13.13 ($3Mn^{2+}$)	13.13 ($3Mn^{2+}$)
C_{cal}^{V} (emu K/mol)	1.50 ($4V^{4+}$)	1.50 ($4V^{4+}$)	2.03 ($V^{3+} + 3V^{4+}$)

[a]Expected Curie constants of hypothetical localized Mn spins (C_{cal}^{Mn}) at the A′ site and V spins (C_{cal}^{V}) at the B site are also listed.

NMVO are highly frustrated. CMVO and LMVO, on the other hand, clearly show antiferromagnetic-like transitions with Néel temperatures of 54 and 44 K, respectively.

It would be interesting at this point to recall the magnetic behaviors in other A-site-ordered perovskite-structure compounds with Mn at the A′ site. In $LaMn_3Mn_4O_{12}$, for example, the B-site Mn^{3+} spins order antiferromagnetically at 78 K, while the A′-site Mn^{3+} spins order antiferromagnetically at 21 K.[19,20] In $LaMn_3Cr_4O_{12}$, the B-site Cr^{3+} spins align antiferromagnetically at 150 K, while the antiferromagnetic transition of the A′ site of Mn^{3+} spins occurs at 50 K.[21] Therefore, the magnetic sublattices of the A′-site Mn and B-site spins do not seem to correlate, and each sublattice shows independent magnetic ordering. In the present $AMn_3V_4O_{12}$, however, we see only a single magnetic transition in each sample. Another possibility would seem to be a ferromagnetic or antiferromagnetic (ferrimagnetic) coupling between the A′-site and B-site spin sublattices, but this can be ruled out because we did not see any ferromagnetic (ferrimagnetic) magnetizations below the transition temperatures. We thus speculate that either the A′-site Mn spin or the B-site V spin sublattice orders at low temperature. Table 2 lists the paramagnetic Curie constants expected from the spins of each sublattice, C_{cal}, of $Na^{+}Mn^{2.33+}{}_3V^{4+}{}_4O_{12}$, $Ca^{2+}Mn^{2+}{}_3V^{4+}{}_4O_{12}$, and $La^{3+}Mn^{2+}{}_3V^{3.75+}{}_4O_{12}$. Let us consider the average of the localized spins of the typical valence states such as Mn^{2+} (high-spin configuration), Mn^{3+} (high-spin configuration), V^{3+}, and V^{4+} for the mixed valence states. Comparing the calculated values with the experimentally observed ones, the spins of only the A′-site Mn appear to contribute to the Curie–Weiss behaviors at high temperature. The results thus strongly suggest that the electrons of the A′-site Mn ions are localized and contribute to the magnetic properties, whereas those of the B-site V ions are delocalized and give a rather large χ_0 in the magnetic susceptibility.

Considering that the spins of only the Mn ions at the A′ site contribute to the magnetic properties, the magnetic transitions observed in CMVO and LMVO should be attributed to the antiferromagnetic ordering of Mn^{2+} spins at A′ sites. The fact that the distance between Mn^{2+} ions is shorter in CMVO than in LMVO (see Table 1) explains why the antiferromagnetic Néel temperature in CMVO (54 K) is higher than that in LMVO (44 K). On the other hand, the spin-glass-like behavior observed in NMVO can be ascribed to randomly distributed Mn^{2+} and Mn^{3+} ions in the A′-site sublattice. Magnetic interactions of Mn^{2+}–Mn^{2+}, Mn^{3+}–Mn^{3+}, and Mn^{2+}–Mn^{3+} in the cubic sublattice should result in glass-like behavior at low temperature. A similar spin-glass-like magnetic behavior was exhibited in $LaMn_3Ti_4O_{12}$, in which the mixed valence state of Mn also led to localized spins of Mn^{+} and Mn^{2+} at the A′ site.[21]

The observed transport properties of $AMn_3V_4O_{12}$ (Figure 5) are consistent with the above magnetic properties. The

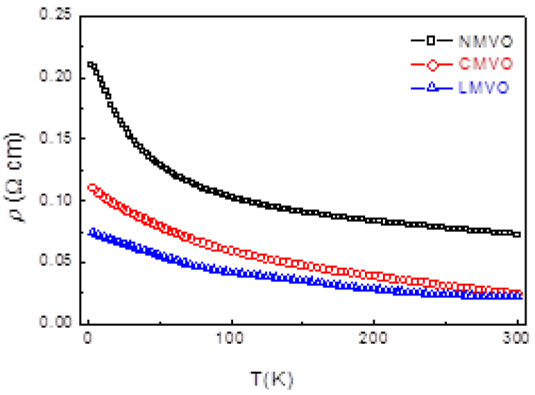

Figure 5. Temperature dependence of resistivity ρ of NMVO, CMVO, and LMVO.

resistivities of the samples are quite low (ρ_{300K} = 0.02 ∼ 0.10 Ω cm) and almost temperature independent. This appears to result from the delocalization of electrons at the B-site V ions, although some grain boundary effects may prevent the samples from having the metallic behavior. Moreover, the samples show no significant changes in either the resistivity at the magnetic transition temperatures or the apparent magnetoresistance. The delocalized electrons of V at the B site do not seem to correlate with magnetic spins of Mn at the A′ site.

The results of the structural, magnetic, and transport measurements have revealed an unusual site-selective doping effect and corresponding changes in the properties of $AMn_3V_4O_{12}$. In the process of changing the A-site ions from Na^{+} to Ca^{2+} and from Ca^{2+} to La^{3+}, the electrons are first doped into the A′-site Mn, changing $Na^{+}Mn^{2.33+}{}_3V^{4+}{}_4O_{12}$ into $Ca^{2+}Mn^{2+}{}_3V^{4+}{}_4O_{12}$, and are then doped into the B-site V, producing $La^{3+}Mn^{2+}{}_3V^{3.75+}{}_4O_{12}$. This implies that the doping energy involved in changing from Mn^{3+} to Mn^{2+} at the A′ site in the $AMn_3V_4O_{12}$ is lower than that in going from V^{4+} to V^{3+} at the B site, but the doping energy in going from Mn^{2+} to Mn^{+} is much higher than that in going from V^{4+} to V^{3+}. Thus, the difference in doping energy causes the present unusual site-selective doping into the A′ site or B site through the A-site substitution. The doping effect of the A-site substitution is completely different from that in another A-site-ordered perovskite with V at the B site, $ACu_3V_4O_{12}$ (A = Na^{+}, Ca^{2+}, and Y^{3+}), in which electrons are doped into both the A′-site Cu and the B-site V. The effect is also different from those in $ACu_3Mn_4O_{12}$ and $ACu_3Fe_4O_{12}$, where the A-site substitution causes doping only at the B-site ions. Another important feature of the present $AMn_3V_4O_{12}$ is that the electrons of the A′-site Mn are localized and result in localized spins, whereas those of the B-site V are delocalized and affect the conducting properties of the samples. Such behavior of ions is unusual and has never been observed in other A-site-ordered perovskite-structure oxides. Interestingly, the delocalized electrons at the B-site V do not show any correlations of the localized spins at the A′-site Mn. A similar behavior was recently found in a simple perovskite $MnVO_3$, where the electrons at the B-site V are itinerant and show no correlation to the localized spins at the A-site Mn.[22]

dx.doi.org/10.1021/ja308851f | J. Am. Chem. Soc. XXXX, XXX, XXX–XXX

SUMMARY

New A-site-ordered cubic perovskite-structure compounds, $AMn_3V_4O_{12}$ (A = Na, Ca, and La), were prepared using high-pressure synthesis. A structural study using SXRD and a valence state analysis of XAS results revealed that the charge distributions of the compounds are $Na^{+}Mn^{2.33+}{}_3V^{4+}{}_4O_{12}$, $Ca^{2+}Mn^{2+}{}_3V^{4+}{}_4O_{12}$, and $La^{3+}Mn^{2+}{}_3V^{3.75+}{}_4O_{12}$. In changing the A-site ions from Na^{+} to Ca^{2+} and from Ca^{2+} to La^{3+}, the electrons are doped into the A′-site Mn and then into the B-site V, and thus the site-selective electron doping is induced in the system. Such an unusual site-selective doping effect has never been observed in other A-site-ordered perovskite-structure oxides. The electrons of Mn at the A′ site are localized and contribute to the magnetic properties. The Mn^{2+} spins in CMVO and LMVO give rise to antiferromagnetism, whereas the random distribution of Mn^{2+} and Mn^{3+} spins in NMVO causes spin-glass-like behavior. The electrons of V at the B site, on the other hand, are delocalized and are responsible for the low resistive behavior of the samples. The delocalized electrons at the B-site V do not correlate with the localized spins at the A′-site Mn.

AUTHOR INFORMATION

Corresponding Author

shimak@scl.kyoto-u.ac.jp

Notes

The authors declare no competing financial interest.

ACKNOWLEDGMENTS

We thank K. Osaka and I. Hirosawa for help with synchrotron X-ray diffraction measurements at BL19B2 in SPring-8. The experiments in SPring-8 were performed with the approval of the Japan Synchrotron Radiation Research Institute. This work was partly supported by Grants-in-Aid for Scientific Research (nos. 19GS0207 and 22740227) and by a grant for the Joint Project of Chemical Synthesis Core Research Institutions from the Ministry of Education, Culture, Sports, Science, and Technology of Japan. This work was also supported by Japan Science and Technology Agency, CREST.

REFERENCES

(1) Imada, M.; Fujimori, A.; Tokura, Y. *Rev. Mod. Phys.* **1998**, *70*, 1039.
(2) Dagotto, E. *Nanoscal Phase Separation and Colossal Magnetoresistance*; Springer-Verlag: Berlin, 2002.
(3) Vasil'ev, A. N.; Volkova, O. S. *Low Temp. Phys.* **2007**, *33*, 895.
(4) Shimakawa, Y. *Inorg. Chem.* **2008**, *47*, 8562.
(5) Zeng, Z.; Greeblatt, M. *Phys. Rev. Lett.* **1998**, *82*, 3164.
(6) Alonso, J. A.; Sánchez-Benítez, J.; De Andrés, A.; Martínez-Lope, M. J.; Casais, M. T.; Martínez, J. L. *Appl. Phys. Lett.* **2003**, *83*, 2663.
(7) Takata, K.; Yamada, I.; Azuma, M.; Takano, M.; Shimakawa, Y. *Phys. Rev. B* **2007**, *76*, 024429.
(8) Yamada, I.; Takata, K.; Hayashi, N.; Shinohara, S.; Azuma, M.; Mori, S.; Muranaka, S.; Shimakawa, Y.; Takano, M. *Angew. Chem., Int. Ed.* **2008**, *47*, 7032.
(9) Long, Y. W.; Hayashi, N.; Saito, T.; Azuma, M.; Muranaka, S.; Shimakawa, Y. *Nature* **2009**, *485*, 60.
(10) Long, Y. W.; Saito, T.; Tohyama, T.; Oka, K.; Azuma, M.; Shimakawa, Y. *Inorg. Chem.* **2009**, *48*, 8489.
(11) Chen, W.-T.; Saito, T.; Hayashi, N.; Takano, M.; Shimakawa, Y. *Sci. Rep.* **2012**, *2*, 449.
(12) Shiraki, H.; Saito, T.; Azuma, M.; Shimakawa, Y. *J. Phys. Soc. Jpn.* **2008**, *77*, 064705.
(13) Larson, A. C.; Von Dreele, R. B. *Los Alamos National Laboratory Report LAUR*; Los Alamos National Laboratory: NM, 2004; pp 86–784.
(14) Toby, B. H. *J. Appl. Crystallogr.* **2001**, *34*, 210.
(15) Abbate, M.; Pen, H. F.; Czyżyk, M. T.; de Groot, F. M. F.; Fuggle, J. C.; Ma, Y. J.; Chen, C. T.; Sette, F.; Fujimori, A.; Ueda, Y.; Kosuge, K. *J. Electron Spectrosc. Relat. Phenom.* **1993**, *62*, 185.
(16) Pen, H. F.; Abbate, M.; Fujimori, A.; Tokura, Y.; Eisaki, H.; Uchida, S.; Sawatzky, G. A. *Phys. Rev. B* **1999**, *59*, 7422.
(17) Gilbert, B.; Frazer, B. H.; Belz, A.; Conrad, P. G.; Nealson, K. H.; Haskel, D.; Lang, J. C.; Srajer, G.; De Stasio, G. *J. Phys. Chem. A* **2003**, *107*, 2839.
(18) Binder, K.; Young, A. P. *Rev. Mod. Phys.* **1986**, *58*, 801.
(19) Prodi, A.; Gilioli, E.; Cabassi, R.; Bolzoni, F.; Licci, F.; Huang, Q. Z.; Lynn, J. W.; Affronte, M.; Gauzzi, A.; Marezio, M. *Phys. Rev. B* **2009**, *79*, 085105.
(20) Imamura, N.; Karppinen, M.; Motohashi, T.; Fu, D. S.; Itoh, M.; Yamauchi, H. *J. Am. Chem. Soc.* **2008**, *130*, 14948.
(21) Long, Y. W.; Saito, T.; Mizumaki, M.; Agui, A.; Shimakawa, Y. *J. Am. Chem. Soc.* **2009**, *131*, 16244.
(22) Markkula, M.; Arevalo-Lopez, A. M.; Kusmartseva, A.; Rodgers, J. A.; Ritter, C.; Wu, H.; Attfield, J. P. *Phys. Rev. B* **2011**, *84*, 094450.